

Figure S1

Fig. S1. Flotillin upregulation induces EMT in the NMuMG non-tumoral murine epithelial mammary cell line.

A) Lysates of NMuMG cells that stably express mCherry (NMuMGmCh) or both flotillin 1-HA and flotillin 2-mCherry (NMuMGF1F2) were analyzed by western blotting using antibodies against flotillin 1 and flotillin 2. In NMuMGF1F2 cells, flotillin levels were comparable to those detected in the invasive mammary tumor MDA-MB-231 cell line. Lysates from MDA-MB-231shFlot2 cells (generated using a shRNA against *FLOT2* to knockdown both flotillins¹⁸) also were analyzed. Actin was used as loading control.

B) Confocal images showing that endogenous flotillin 1 and 2 are localized at the plasma membrane in NMuMGmCh cells. In NMuMGF1F2 cells, they translocate to vesicular compartments, where they co-localize, as previously shown in MCF10AF1F2 and in MDA-MB-231 cells¹⁸.

C) Confocal images showing the co-localization of flotillin 1-HA and flotillin 2-mCherry in intracellular vesicles in NMuMGF1F2 cells.

D) RT-qPCR analysis of the mRNA levels of E-cadherin, N-cadherin and vimentin in NMuMGmCh and NMuMGF1F2 cells. Histograms show the mean \pm SEM of 4 independent experiments.

E, M) Western blots performed using NMuMGmCh and NMuMGF1F2 cell lysates to compare the amount of E- and N-cadherin (E), and ZEB1 (M). Histograms show the mean \pm s.e.m. of at least 4 independent experiments.

F, G) Comparison of the distribution of endogenous E-, N-cadherin (F), and ZO-1 and vimentin (G) in NMuMGmCh and NMuMGF1F2 cells analyzed by immunofluorescence. Nuclei are stained with Hoechst (Hst, blue).

H) Scanning electron microscopy images of the monolayer formed by NMuMGmCh and NMuMGF1F2 cells.

I, J) F-actin cytoskeleton organization in NMuMGmCh and NMuMGF1F2 cells (I) and in MCF10AmCh and MCF10AF1F2 cells (J). Confluent cells were fixed and stained for F-actin (green) using Alexa488-Phalloidin. Nuclei (blue) were stained with Hoechst (flotillin2-mCherry signal is shown in the bottom panels). **(I)** Z-projection and 3D surface reconstruction of NMuMGmCh and NMuMGF1F2 cells was performed with 35 plans and 22 plans every 0.3 μ m for NMuMGmCh and NMuMGF1F2 cells, respectively. **(J)** A stack of images was acquired by confocal microscopy (26 and 21 plans every 0.2 μ m for MCF10AmCh and MCF10AF1F2 cells, respectively). The shown X-Y image corresponds to one single plane passing through the apical/top of the cell. X-Z and Y-Z projections along the indicated axes are shown.

K, L) *Characterization of the transcriptional repressors of E-cadherin expression.* RT-qPCR analysis of the mRNA levels of Snail1, Snail2, TWIST in MCF10AmCh and MCF10AF1F2 cells (K) and Zeb1 and 2 in NMuMGmCh and NMuMGF1F2 cells (L). Histograms show the mean \pm s.e.m. of 4 independent experiments.

N) Confocal images of ZEB1 localization and nuclei stained with Hoechst (Hst, blue) in NMuMGmCh and NMuMGF1F2 cells.

Images in B, C, F, G, I, J and N are representative of cells observed in at least 3 independent experiments Scale bars: 10 μ m.

*P<0.05 and **P<0.01 were determined with the Mann-Whitney test, two-tailed P-values (D, E, L, M).

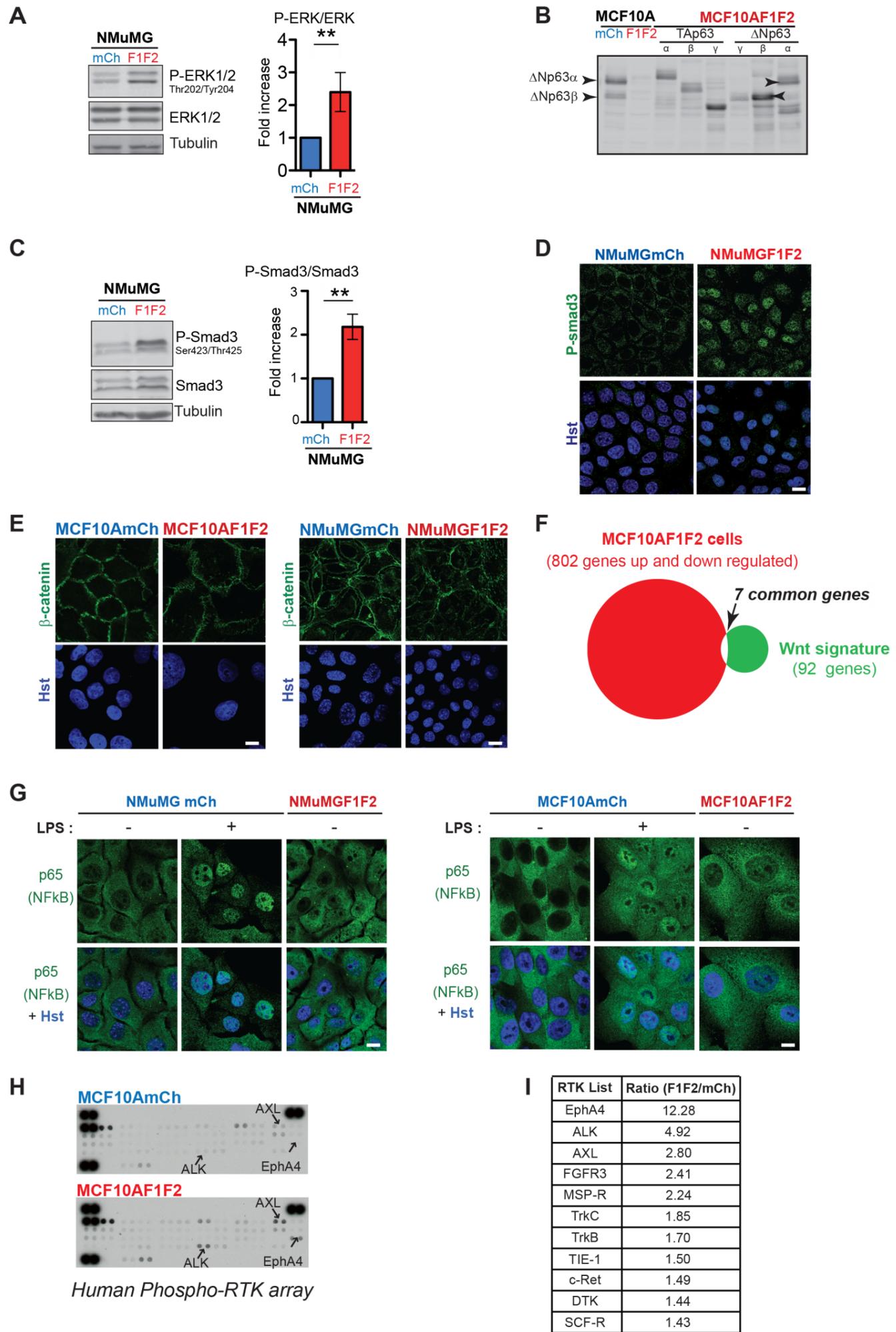


Figure S2

Fig. S2. Determination of the p63 isoforms expressed in MCF10AmCh cells and downregulated in MCF10AF1F2 cells. Identification of non-activated signaling pathways downstream of flotillin upregulation in mammary epithelial cells. Screening for activated RTKs upon flotillin upregulation.

A, C) Cell lysates from NMuMGmCh and NMuMGF1F2 cells were analyzed by western blotting to evaluate the phosphorylation status of ERK1/2 (B) and SMAD3 (C). Histograms (mean \pm s.e.m. of 4 independent experiments) show the quantification of the phosphorylation signal normalized to the total amount of each protein.

B) *Characterization of the p63 isoforms expressed in MCF10AmCh and MCF10AF1F2 cells.* Western blot analysis of the p63 isoforms in lysates from MCF10AmCh, MCF10AF1F2 and MCF10AF1F2 cells transfected with different non-tagged p63 isoforms (TAp63 γ , β , α or Δ Np63 γ , β , α) using an antibody against all p63 isoforms. Δ Np63 α and to a lesser extent Δ Np63 β are the two main isoforms expressed in MCF10A cells. The expression of Δ Np63 α and of Δ Np63 β was abolished in MCF10AF1F2 cells (as shown in fig. 2G).

D) NMuMGmCh and NMuMGF1F2 cells were labeled with an antibody against SMAD3 phosphorylated on S423/425 and with Hoechst (Hst).

E, F, G) *The oncogenic NF- κ B and WNT canonical signaling pathways are not activated following flotillin upregulation in MCF10A and NMuMG cells.* **E)** β -catenin distribution, analyzed by immunofluorescence is similar in MCF10AmCh and MCF10AF1F2 cells and in NMuMGmCh and NMuMGF1F2 cells, and no nuclear staining was detected, indicating that the WNT canonical pathway is not activated. Nuclei are stained with Hoechst (Hst). **F)** Venn diagrams illustrating the small overlap between the 802 differentially expressed genes identified by RNA-seq in MCF10AF1F2 cells versus MCF10AmCh cells and the 92 differentially expressed genes of an established WNT signature (http://web.stanford.edu/group/nusselab/cgi-bin/wnt/target_genes). Only 7/92 genes overlapped. **G)** Cellular distribution of the NF- κ B p65 subunit, analyzed by immunofluorescence, in MCF10AmCh and MCF10AF1F2 cells and in NMuMGmCh and NMuMGF1F2 cells. In all cases, NF- κ B p65 was excluded from the nucleus, indicating that the NF- κ B pathway is not activated upon flotillin upregulation. As positive control, MCF10AmCh cells and NMuMGmCh cells were stimulated with lipopolysaccharide (LPS; 1 μ g/ml, 1h) to induce NF- κ B p65 translocation to the nucleus.

H) Flotillin upregulation increases the phosphorylation level of several RTKs. Human phospho-Receptor Tyrosine kinase arrays were incubated with 200 μ g of MCF10AmCh or MCF10AF1F2 cell lysates (cultured in the presence of serum) and processed as described by the manufacturer. One array example is shown.

I) List of the 11 RTKs with the highest increase in phosphorylation in MCF10AF1F2 compared with MCF10AmCh cells (data from 2 independent experiments).

Images in D, E, G are representative of at least 3 independent experiments. Scale bars: 10 μ m.

**P<0.01 was determined with the Mann-Whitney test, two-tailed P-values (A, C).

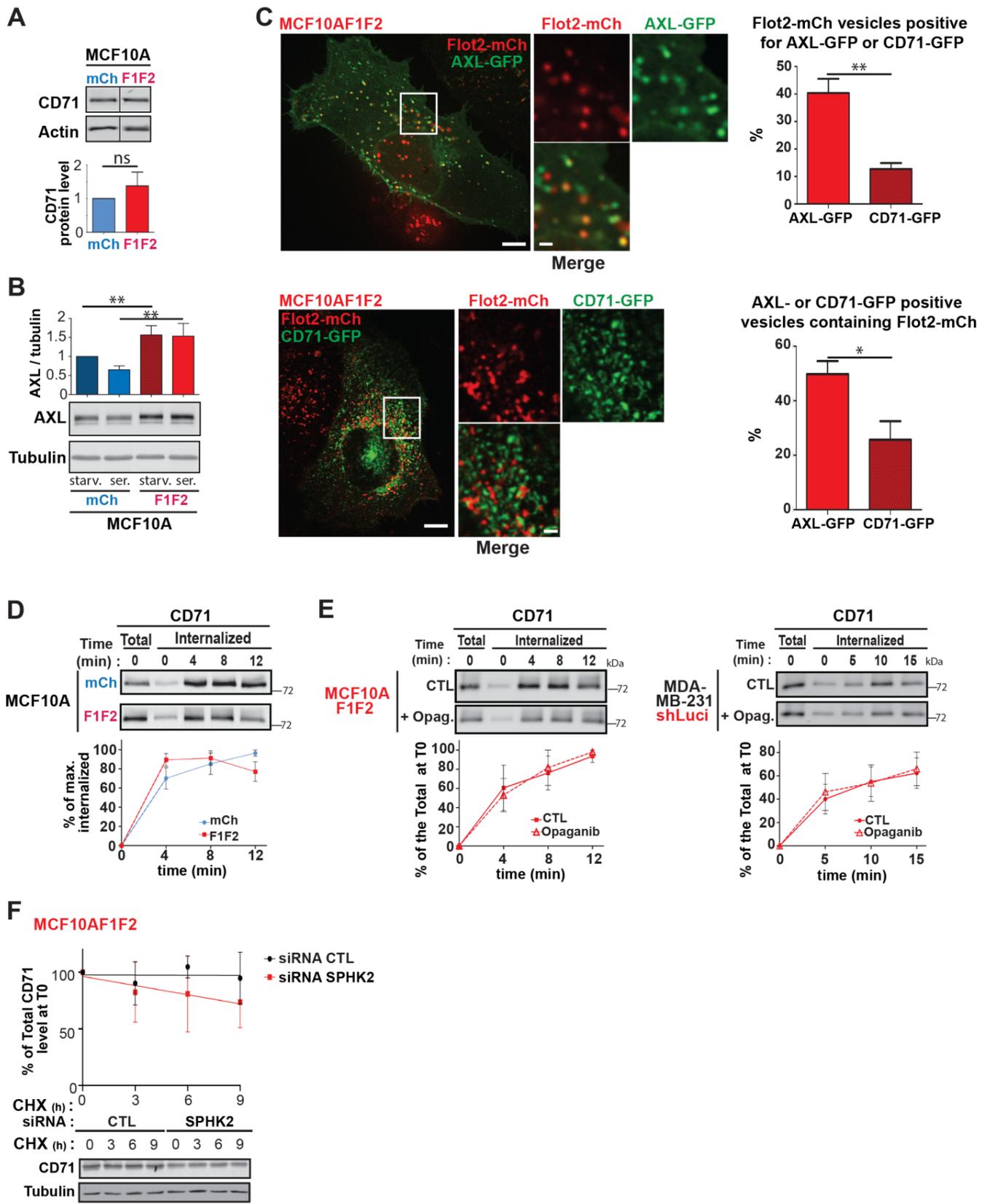


Figure S3

Fig. S3. The transferrin receptor CD71 is not a cargo of the UFIT pathway.

A) Flotillin upregulation does not affect CD71 level. Cell lysates of MCF10AmCh and MCF10AF1F2 cells were probed by western blotting with antibodies against CD71 and actin. Results are expressed as fold-change compared with MCF10AmCh cells and are the mean \pm s.e.m. of 4 independent experiments.

B) Flotillin upregulation promotes AXL protein level increase independently of serum stimulation. Lysates from MCF10AmCh and MCF10AF1F2 cells, serum-starved for 16h (starv.) or maintained in the presence of serum (ser.), were probed by western blotting with antibodies against AXL and tubulin. Results are expressed as fold-change compared with MCF10AmCh cells in serum-starved conditions and are the mean \pm s.e.m. of 5 independent experiments.

C) The transferrin receptor CD71 poorly localizes in flotillin-positive late endosomes compared with AXL. Live MCF10AF1F2 cells that express CD71-GFP or AXL-GFP were imaged by spinning disk confocal microscopy. Images are representative of several cells in 3 independent experiments. Scale bars: 10 μ m in the main image and 2 μ m in the magnified images from the boxed area. The histograms show the percentage of Flotillin2-mCherry (Flot2-mCh)-positive vesicles containing AXL-GFP or CD71-GFP (upper histogram), and the percentage of AXL-GFP- or CD71-GFP-positive vesicles containing Flot2-mCh (lower histogram). Results are the mean \pm s.e.m. (n=690 Flot2-mCh-positive vesicles and n=746 AXL-GFP labeled vesicles in 21 AXL-GFP-expressing MCF10AF1F2 cells; and n=1511 Flot2-mCh-positive vesicles and n=1207 AXL-GFP labeled vesicles in 20 CD71-GFP-expressing MCF10AF1F2 cells).

D) Flotillin upregulation does not affect the transferrin receptor endocytosis. Kinetics of CD71 (transferrin receptor) internalization in MCF10AmCh and MCF10AF1F2 cells analyzed in the same experiments presented in figure 4G. Surface proteins were labeled with biotin at 4°C and cells were incubated at 37°C for the indicated times to allow endocytosis. CD71 presence in the internalized biotinylated fraction was analyzed by western blotting using relevant antibodies, and quantified as the percentage of the maximum level of internalized protein. Results are expressed as the mean \pm s.e.m. of 4 independent experiments. The CD71 internalization rates were not significantly different between cell lines at 4, 8 and 12 min.

E) SPHK2 inhibition has no impact on CD71 internalization in flotillin-upregulated cells. Kinetics of CD71 internalization in MCF10AF1F2 and in MDA-MB-231shLuci cells untreated (CTL) or pre-treated with Opaganib (50 μ M, 4h), as in figure 6G and H. Surface proteins were labeled with biotin at 4°C, and cells were incubated at 37°C for the indicated times to allow endocytosis. Opaganib was maintained throughout the experiments. CD71 presence in the internalized biotinylated fraction was probed by western blotting using relevant antibodies. Results are expressed as the percentage of the maximum level of CD71 surface level at T0 and are the mean \pm SEM of 4 independent experiments. CD71 internalization rates were not significantly different between control and Opaganib-treated cells in both cell lines. Simple linear regression analysis with GraphPad Prism did not detect any difference between the curves (p=0.77 for MCF10AF1F2 cell and P=0.96 for MDA-MB-231 cells)

F) In contrast to AXL (fig. 6G), CD71 internalization rate is not modified by SPHK2 knock-down. MCF10AF1F2 cells were transfected with siRNAs against luciferase (CTL) or SPHK2 for 72 hours, incubated with cycloheximide (CHX, 100 μ g/ml), and the cell lysates were collected at the indicated time points. CD71 levels were assessed by western blot analysis. The graph shows the level of CD71 expressed as the percentage of the total level at T0. The results are the mean \pm s.e.m. of 4 independent experiments. Simple linear regression analysis with GraphPad Prism did not detect any was established under each condition. According to Graph Pad Prism, the slopes of the curves obtained for each condition were not considered as significantly different between conditions (P=0.1236).

*P<0.05 and **P<0.01 were determined with the Mann-Whitney test, two-tailed P-values (A, B, C)

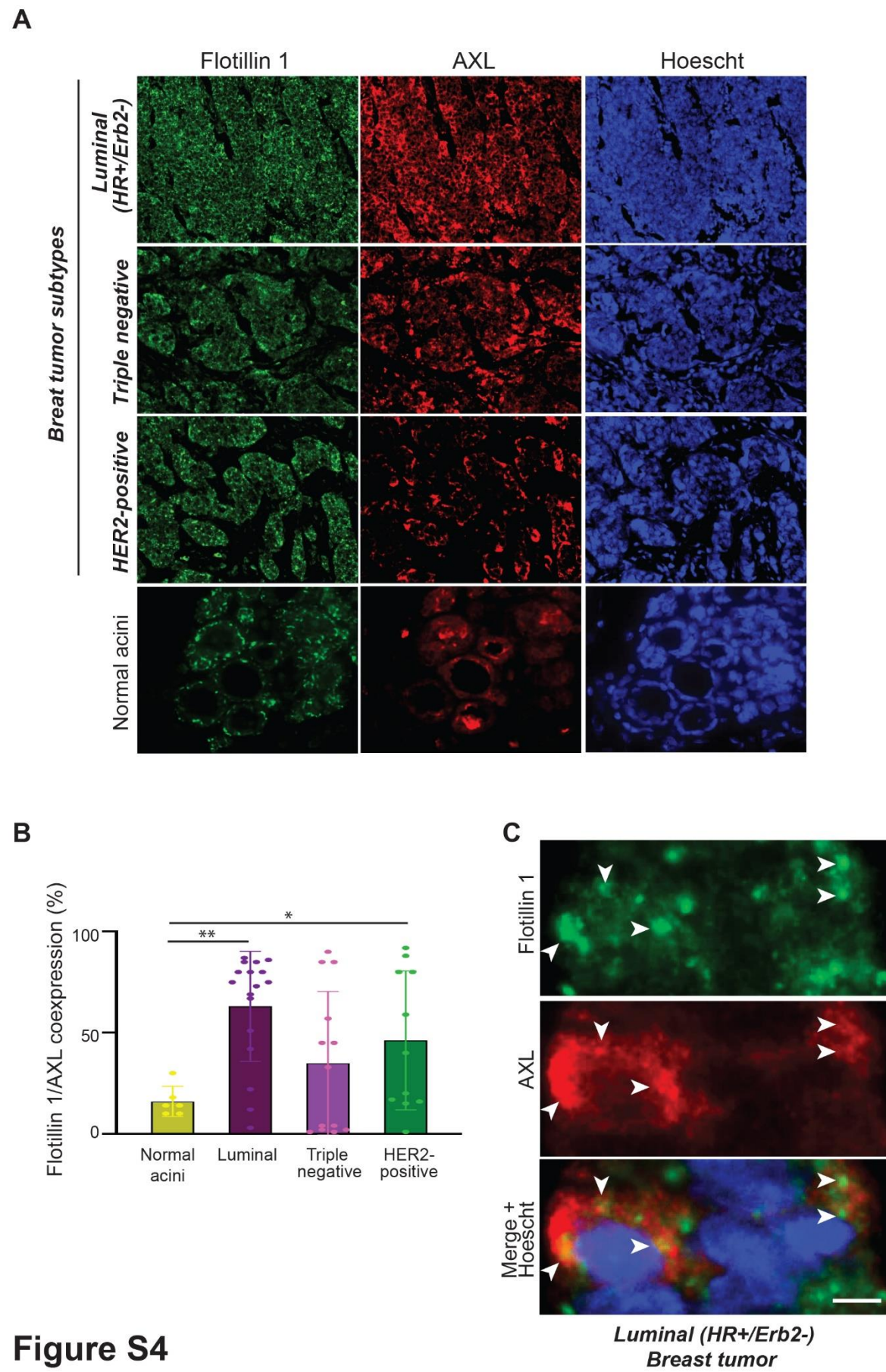


Figure S4

Fig. S4. Flotillin 1 and AXL are co-expressed in invasive breast tumor cells.

A) Immunofluorescence analysis of flotillin 1 and AXL in invasive breast tumor tissue sections in one patient sample for each breast tumor subtype and in non-tumoral breast tissue. Nuclei were stained with DAPI. Scale bar: 10 μ m.

B) Immunofluorescence analysis of flotillin 1 and AXL expression in 6 non-tumoral breast tissue samples and 43 breast tumor samples (Luminal n= 17, Triple Negative n =15, HER2⁺ =11). Co-expression was calculated in the different subtypes with the Vectra 3.0 Automated Quantitative Pathology Imaging System. Results show the mean \pm s.e.m.

C) High magnification immunofluorescence images of flotillin 1 and AXL expression in a luminal B invasive breast tumor section. Nuclei were stained with Hoechst. Arrows indicate flotillin 1 and AXL colocalization in intracellular vesicles. Scale bar: 10 μ m.

*P<0.05 and **P<0.01 were determined with the Mann-Whitney test, two-tailed P-values (B)

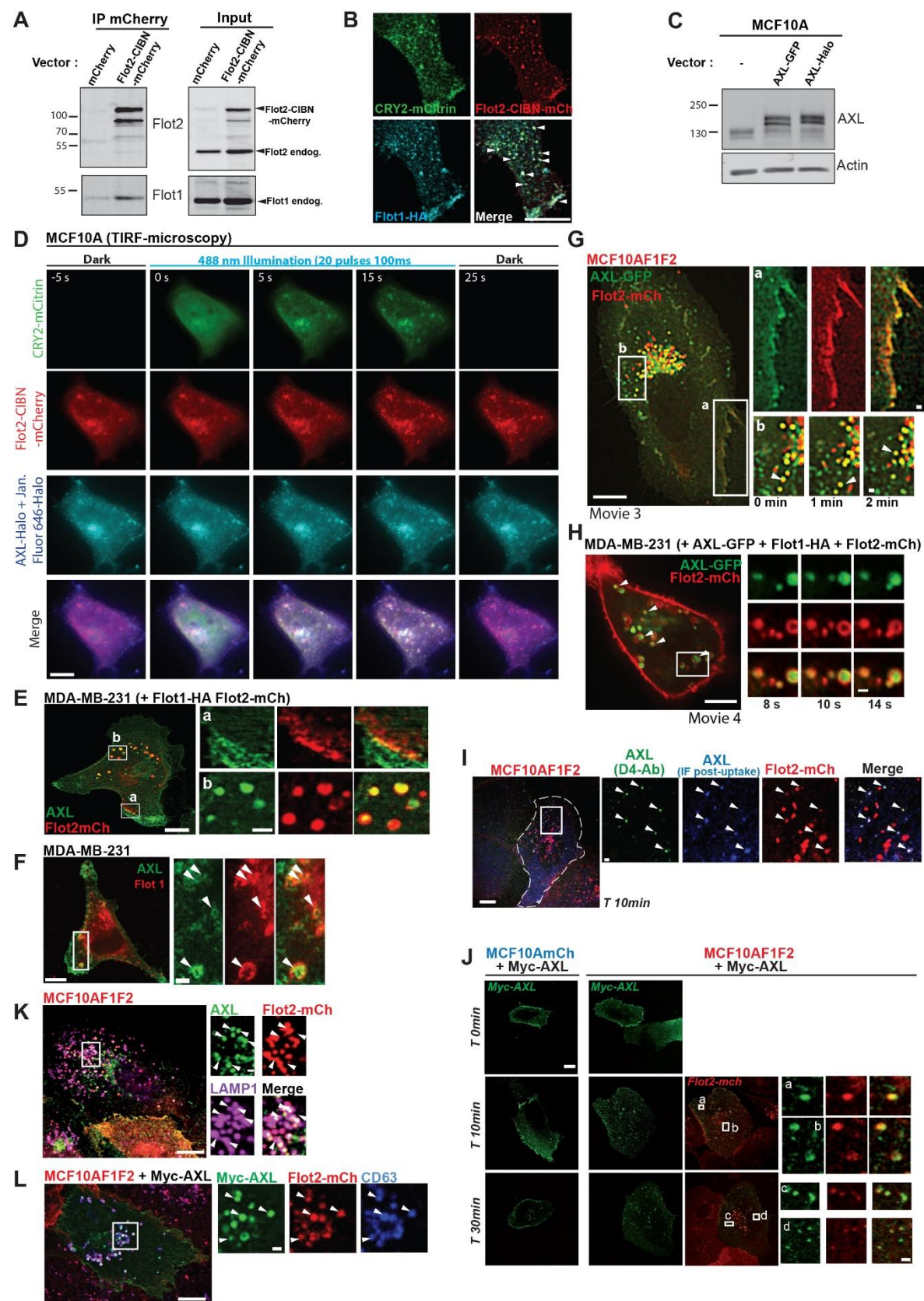


Figure S5

Fig. S5. Co-distribution of AXL and flotillins at the plasma membrane and in late endosomes.

A) Flotillin2-CIBN-mCherry interacts with flotillin 1. Immunoprecipitations using an antibody against mCherry (mCherry trap) and lysates from MCF10A cells that express mCherry alone or flotillin 2-CIBN-mCherry. Immunoprecipitates were then analyzed with antibodies to detect flotillin 1 and 2. Flotillin 1 was co-immunoprecipitated only in lysates from cells that express flotillin 2-CIBN-mCherry, but not mCherry alone. Results are representative of 3 independent experiments.

B) Light-induced flotillin 2-CIBN-mCherry microdomains contain flotillin 1. MCF10A cells that co-express flotillin 2-CIBN-mCherry, flotillin 1-HA and CRY2-mCitrin were illuminated at 488 nm for 1 min, fixed, incubated with an anti-HA antibody and imaged by confocal microscopy. CRY2-mCitrin patches containing flotillin 2-CIBN-mCherry (white arrows) also exhibit flotillin 1-HA signal. Results are representative of 3 independent experiments.

C) Characterization of the AXL-GFP and AXL-Halo constructs. MCF10A cells were transfected with empty vector (-) or plasmids encoding AXL-GFP or AXL-Halo. Expression of the proteins of the expected size (138+28=166 kDa for AXL-GFP) and (138+28=171 kDa for AXL-Halo) is shown. A doublet was observed for each tagged protein like for endogenous AXL.

D) Still images from a TIRF-microscopy video of one MCF10A cell that co-expresses CRY2-mCitrin, flotillin 2-CIBN-mCherry and AXL-Halo labeled with Halo-Tag-Janelia Fluor 646. The cell was imaged before, during, and after 488 nm illumination (22 pulses of 100 ms each every second). Merged signals in the same cell 15 s after starting the 488 nm illumination is shown in Fig. 4B.

E, F) Distribution and colocalization of endogenous AXL with flotillins in MDA-MB-231 cells analyzed by confocal microscopy after immunofluorescence staining. (E) The cell expresses flotillin 2-mCherry. Higher magnification images of the two boxed regions show AXL colocalization with flotillin 2-mCherry at the plasma membrane (a) and in intracellular vesicles (b). (F) Endogenous flotillin 1 was detected by immunocytochemistry. The boxed region shows AXL colocalization with flotillin 1 in intracellular vesicles.

G) Co-trafficking of AXL and flotillins in MCF10AF1F2 cells. Still images of a representative time-lapse series (movie 3) of a MCF10AF1F2 cell that expresses AXL-GFP to illustrate the co-localization of AXL-GFP and flotillin 2-mCherry at the plasma membrane (box a), and in intracellular vesicles (box b) and their co-trafficking. The white arrow allows following one vesicle over time.

H) Co-trafficking of AXL and flotillins in MDA-MB-231 cells. MDA-MB-231 cells were transfected with AXL-GFP, flotillin 2-mCherry and flotillin 1-HA-encoding plasmids. Live cells were imaged by spinning disk confocal microscopy. Three images from the boxed region, acquired at different times, show the co-trafficking of AXL-GFP and flotillin 2-mCherry in intracellular vesicles (movie 4).

I) An MCF10AF1F2 cell (the same cell as shown in Fig. 4F) was incubated with the anti-AXL D4 antibody (against AXL extracellular domain) at 4°C followed by incubation at 37°C for 10 min to allow AXL internalization. After fixation and permeabilization, internalized AXL was labeled (green) with a FITC-conjugated secondary antibody against the D4 antibody. Immunofluorescence staining of AXL (blue) was also performed using an antibody against AXL cytoplasmic domain and an Alexa-633 conjugated secondary antibody. Arrowheads indicate flotillin 2-mCherry-positive vesicles in which AXL is internalized (green).

J) MCF10AmCh and MCF10AF1F2 cells that express Myc-tagged AXL were incubated with an anti-Myc antibody at 4°C, followed by incubation at 37°C for the indicated times. Myc-AXL distribution was analyzed by immunocytochemistry using an Alexa488-conjugated secondary antibody.

K) In MCF10AF1F2 cells, endogenous AXL is localized in flotillin 2-mCherry vesicles positive for the endolysosomal marker LAMP1 (confocal microscopy image).

L) Myc-tagged AXL expressed in MCF10AF1F2 cells is localized in flotillin 2-mCherry vesicles positive for the late endosomal marker CD63 (Confocal microscopy image after immunofluorescence). Images shown in B, D - K are representative of 3 to 5 independent experiments. In E, F, G, H, I, J, K and L scale bars = 10 µm in the main images and = 2 µm in the magnified images from the insets.

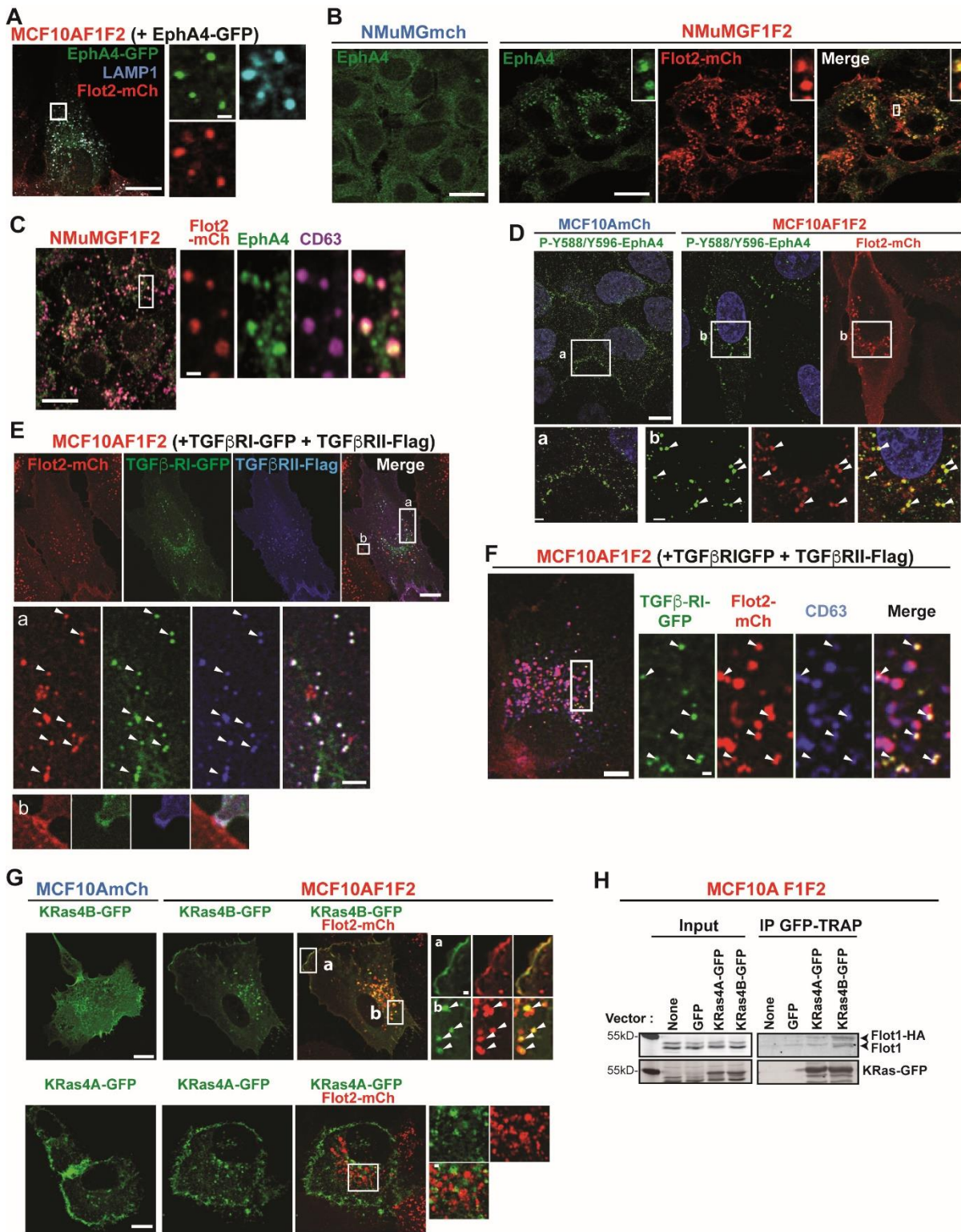


Figure S6

Fig. S6. The RTK EphA4, the TGF η receptors, and Kras4B are located in flotillin-positive late endosomes.

A) Confocal microscopy image of one MCF10AF1F2 cell that expresses EphA4-GFP and stained for LAMP1, showing flotillin 2/EphA4 co-localization in LAMP-1-positive vesicles.

B, C) Immunofluorescence analysis of NMuMGmCh and NMuMGF1F2 cells to detect endogenous EphA4. In NMuMGF1F2 cells, EphA4 relocates in intracellular vesicles, many of which are flotillin 2-mCherry- and CD63-positive (C).

D) MCF10AmCh and MCF10AF1F2 cells were analyzed by immunofluorescence using an antibody against EphA4 phosphorylated on Y588/Y596. In MCF10AmCh cells the signal is at cell-cell contacts (magnified image from the boxed area (a)), whereas it is concentrated in intracellular vesicles in MCF10AF1F2 cells where it co-localizes with flotillin 2-mCherry (magnified images from boxed areas (b)).

E) MCF10AF1F2 cells that co-express the TGF β -RI (GFP-tagged) and TGF β -RII (Flag-tagged) subunits were analyzed by immunofluorescence using an anti-Flag antibody and imaged by confocal microscopy. Both subunits are concomitantly found at the plasma membrane and in intracellular vesicles (white arrows) where they colocalize with flotillin 2-mCherry.

F) MCF10AF1F2 cells that co-express TGF β -RI-GFP and TGF β -RII-Flag were stained for CD63 and imaged by confocal microscopy. White arrows in the magnified images of the boxed area indicate co-localization of TGF β -RI-GFP, CD63 and flotillin 2-mCherry in intracellular vesicles. Scale bars= 10 μ m in the main images and =1 μ m in the magnified regions.

G) *Flotillin upregulation specifically relocates K-Ras4B to flotillin-positive endosomes.* Confocal images of MCF10AmCh and MCF10AF1F2 cells that express K-Ras4A-GFP or K-Ras4B-GFP. Unlike K-Ras4A-GFP (lower panels), K-Ras4B-GFP (upper panels) co-localizes with flotillins and its distribution is modified in MCF10AF1F2 cells compared with MCF10AmCh cells (upper panel). K-Ras4B-GFP is mainly present at the plasma membrane in MCF10AmCh cells. Conversely, in MCF10AF1F2 cells, it remains visible at the plasma membrane where it co-localizes with flotillin 2-mCherry (magnified images from the boxed region (a)), but it is also strongly recruited to flotillin 2-mCherry-positive vesicles and co-trafficked with flotillin 2 (magnified images of the boxed region (b)). In A, B, C, D, E, G, scale bars = 10 μ m in the main images and = 2 μ m in the magnified images from insets. In panels A-G, images are representative of several cells observed in 3 independent experiments.

H) *K-Ras4B forms a complex with flotillin 1.* Lysates from MCF10AF1F2 cells that express GFP alone, K-Ras4A-GFP, or K-Ras4B-GFP were immunoprecipitated with GFP-TRAP. Immunoprecipitates were probed by western blotting using anti-flotillin 1 and anti-pan-Ras antibodies. Both K-Ras isoforms are similarly expressed and immunoprecipitated. The signal for flotillin 1-HA and flotillin 1 in precipitates from K-Ras4B-GFP-expressing cells is clearly higher than the signal observed in precipitates from K-Ras4A-GFP-expressing cells that is similar to the background signal found in precipitates from GFP-expressing cells. Results are representative of 3 independent experiments.

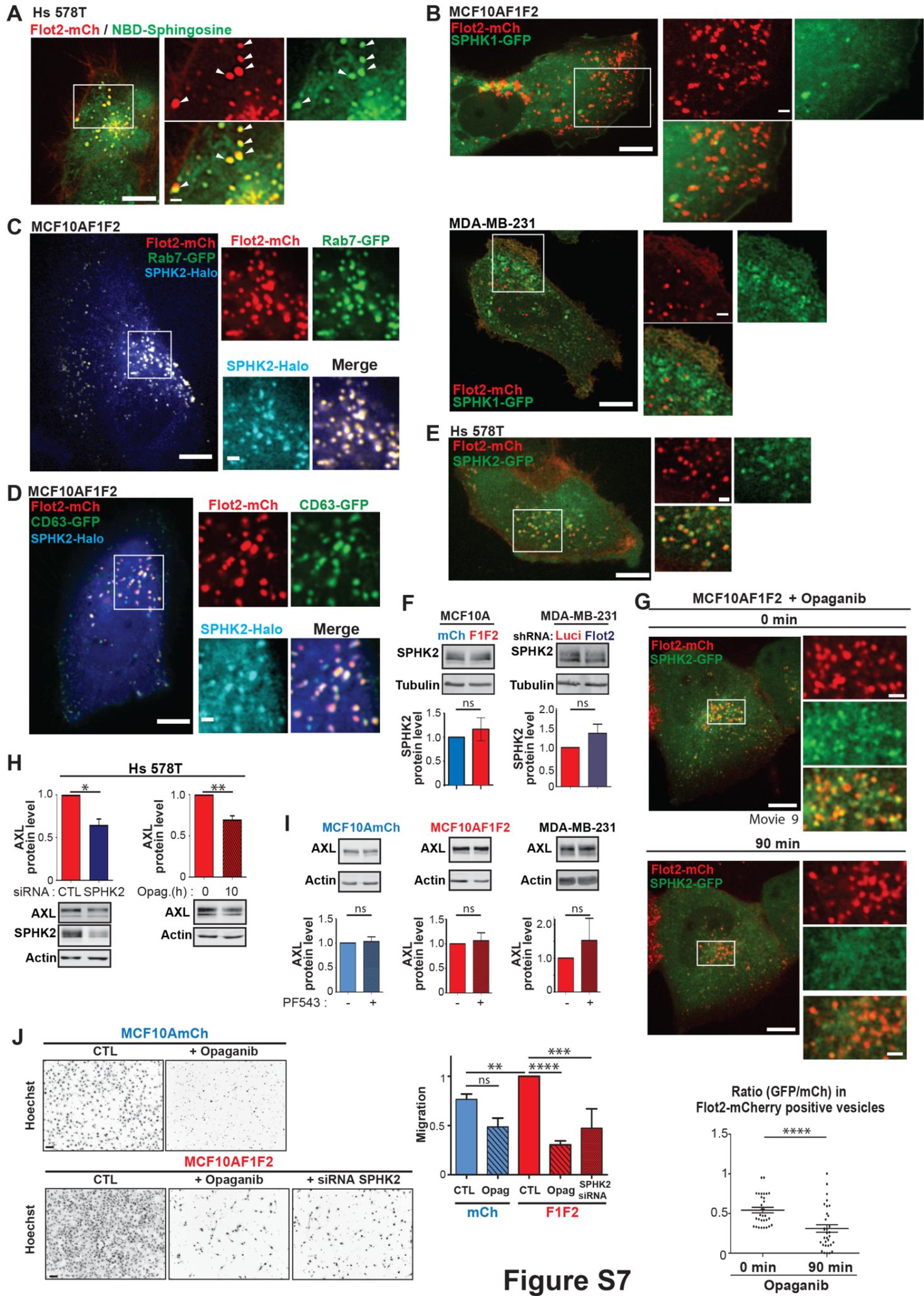


Figure S7

Fig. S7. Sphingosine, SPHK1 and 2 localization and effect of SPHK inhibitors.

A) *NBD-sphingosine accumulates in flotillin-positive late endosomes.* Live Hs 578T cells that express flotillin2-mCherry were incubated with NBD-sphingosine. A still image acquired 5 min after the addition of the fluorescent lipid is shown. White arrows show flotillin 2-mCherry-positive vesicles where NBD-sphingosine accumulates.

B) *SPHK1 is barely detected in flotillin-positive endosomes.* Live MCF10AF1F2 cells that express SPHK1-GFP (left), and MDA-MB-231 cells that co-express flotillin 1-mCherry and SPHK1-GFP (right) were imaged by spinning disk confocal microscopy (see quantification in fig. 5D).

C, D) *SPHK2 colocalizes with flotillins in Rab7- and CD63-positive vesicles.* Still images of live MCF10AF1F2 cells that express SPHK2-Halo labeled with Halo-tag-Janelia Fluor 646 and Rab7-GFP (C), or CD63-GFP (D) imaged by spinning disk confocal microscopy. Images are representative of 3 independent experiments.

E) *SPHK2 is enriched in flotillin-positive late endosomes in Hs 578T cells.* Live Hs 578T cells that co-express flotillin 2-mCherry and SPHK2-GFP were imaged by spinning disk confocal microscopy. Still images are shown

F) *Flotillin level does not modulate SPHK2 protein expression.* SPHK2 and tubulin were assessed in whole cell extracts from MCF10AmCh, MCF10AF1F2, MDA-MB-231shLuci, and MDA-MB-231shFlot2 cells by western blotting using specific antibodies. The histograms show SPHK2 level (normalized to tubulin) expressed as fold-change compared with MCF10AmCh or MDA-MB-231shLuci cells, and data are the mean \pm s.e.m. of 4 independent experiments.

G) *Opaganib induces the delocalization of SPHK2 from flotillin-positive vesicles.* Live MCF10AF1F2 cells that express SPHK2-GFP were imaged right after incubation with opaganib by spinning disk confocal microscopy every 15 min. The SPHK2-GFP signal associated with flotillin 2-mCherry positive vesicles was clearly decreased after 90 min of incubation. The histogram (mean \pm s.e.m.) shows the GFP/mCherry signal ratio in flotillin 2-mCherry-positive vesicles at 0 and after 90 min of opaganib incubation (31 vesicles at T0 and 32 vesicles at T90 from 3 independent cells).

In panels A, B, C, D, E and G, scale bars = 10 μ m in the main images, and to = 2 μ m in the magnified images from the boxed area.

H) *SPHK2-inhibition decreases AXL in Hs 578T cells.* (Left) Hs 578T cells were transfected with siRNAs against luciferase (CTL) or SPHK2. In whole lysates, siRNA efficacy was tested by western blotting with antibodies against SPHK2, AXL and actin. (Right) Hs 578T cells were incubated with opaganib (50 μ M, 10 h). AXL and actin were analyzed by western blotting of whole cell lysates. The histograms show the level of AXL normalized to the actin signal, expressed as fold-change compared with the control condition and are the mean \pm s.e.m. of 4 independent experiments.

I) *SPHK1 inhibition does not influence AXL level in cells in which flotillins are upregulated.* MCF10AmCh, MCF10AF1F2 and MDA-MB-231 cells were incubated with the selective SPHK1 inhibitor PF543 (10 μ M, 24h). AXL and actin levels were measured by western blotting in cell lysates. The histograms show AXL level, expressed as fold-change compared with the control condition (no PF543), and data are the mean \pm s.e.m. of 4 independent experiments.

J) *Boyden chamber migration assay.* MCF10AmCh and MCF10AF1F2 cells were seeded in the top of Boyden chamber inserts in serum-free medium, and serum-containing medium, acting as chemoattractant, was placed in the bottom well. When indicated, opaganib (50 μ M) was added in the upper and lower chambers, or MCF10AF1F2 were transfected with siRNAs against SPHK2 for 48h prior to seeding. Representative inverted-microscopy images of Hoechst-stained nuclei of cells that migrated through the pores. The histogram shows the number of cells that migrated compared with untreated MCF10AF1F2 cells, and data are the mean \pm s.e.m. of at least 4 independent experiments. Scale bar: 50 μ m.

*P<0.05, **P<0.01, ***P<0.001 and ****P<0.0001 were determined with the Mann-Whitney test, two-tailed P-values (F,G,H,I and J)

Table S1. The differential gene expression analysis was processed on three replicates per condition to compare the levels of the transcripts between MCF10AmCh and MCF10AF1F2 cells. Confrontation of the results obtained from the Deseq2 and Tuxedo analyses

Click here to download Table S1

Table S2. List of the enriched GO terms and the enriched pathways obtained from the analysis of the 802 differentially expressed genes between MCF10mCh and MCF10AF1F2 using three distinct bioinformatic tools (KEGG, DAVID, and Genomatix)

KEGG Enrichr pathways	KEGG David	Genomatix
Cell adhesion molecules (CAMs)_Homo sapiens_hsa04514	hsa04151:PI3K-Akt signaling pathway	Extracellular matrix organization
PI3K-Akt signaling pathway_Homo sapiens_hsa04151	hsa04514:Cell adhesion molecules (CAMs)	Cell-Cell communication
Proteoglycans in cancer_Homo sapiens_hsa05205	hsa05205:Proteoglycans in cancer	Cell junction organization
Hematopoietic cell lineage_Homo sapiens_hsa04640	hsa04640:Hematopoietic cell lineage	a6b1 and a6b4 Integrin signaling
Pathways in cancer_Homo sapiens_hsa05200	hsa05200:Pathways in cancer	Beta5 beta6 beta7 and beta8 integrin cell surface interactions
Rap1 signaling pathway_Homo sapiens_hsa04015	hsa04015:Rap1 signaling pathway	amb2 integrin signaling
Malaria_Homo sapiens_hsa05144	hsa05144:Malaria	Alpha6Beta4Integrin
Inflammatory bowel disease (IBD)_Homo sapiens_hsa05321	hsa04060:Cytokine-cytokine receptor interaction	EGFR1
Insulin resistance_Homo sapiens_hsa04931	hsa05321:Inflammatory bowel disease (IBD)	Syndecan-2-mediated signaling events
AGE-RAGE signaling pathway in diabetic complications_Homo sapiens_hsa04933	hsa04931:Insulin resistance	Direct p53 effectors
Ras signaling pathway_Homo sapiens_hsa04014	hsa04014:Ras signaling pathway	FGF signaling pathway
Cytokine-cytokine receptor interaction_Homo sapiens_hsa04060	hsa04512:ECM-receptor interaction	Signaling by MST1
Prion diseases_Homo sapiens_hsa05020	hsa05323:Rheumatoid arthritis	Transport of small molecules
	hsa05230:Central carbon metabolism in cancer	Visual phototransduction
	hsa00601:Glycosphingolipid biosynthesis - lacto and neolacto series	Cytokine Signaling in Immune system
	hsa04750:Inflammatory mediator regulation of TRP channels	SHP2 signaling
	hsa04610:Complement and coagulation cascades	Beta2 integrin cell surface interactions
	hsa05412:Arrhythmogenic right ventricular cardiomyopathy (ARVC)	Angiopoietin receptor Tie2-mediated signaling
	hsa05218:Melanoma	Hemostasis
	hsa05202:Transcriptional misregulation in cancer	Validated transcriptional targets of TAp63 isoforms
	hsa04064:NF-kappa B signaling pathway	ion channels and their functional role in vascular endothelium
	hsa04144:Endocytosis	Signaling by Retinoic Acid
		Beta3 integrin cell surface interactions
		Blood coagulation
		Beta1 integrin cell surface interactions
		Plasminogen activating cascade
		Validated transcriptional targets of deltaNp63 isoforms
		ATF-2 transcription factor network
		Endogenous TLR signaling
		IL27-mediated signaling events
		Validated transcriptional targets of AP1 family members Fra1 and Fra2
		signal transduction through il1r
		inhibition of matrix metalloproteinases
		IL-7
		PI3K/AKT Signaling in Cancer

David version 6.8

<https://david.ncifcrf.gov/home.jsp>

DAVID users may publish or otherwise publicly disclose the results of using DAVID. Please acknowledge DAVID in your publications by citing the following two references:

Huang DW, Sherman BT, Lempicki RA. Systematic and integrative analysis of large gene lists using DAVID Bioinformatics Resources. *Nature Protoc.* 2009;4(1):44-57.

Huang DW, Sherman BT, Lempicki RA. Bioinformatics enrichment tools: paths toward the comprehensive functional analysis of large gene lists. *Nucleic Acids Res.* 2009;37(1):1-13.

KEGG Pathway DataBase

<https://www.kegg.jp/kegg/pathway.html>

Please cite the following article(s) when using KEGG.

Kanehisa, Furumichi, M., Tanabe, M., Sato, Y., and Morishima, K.; KEGG: new perspectives on genomes, pathways, diseases and drugs. *Nucleic Acids Res.* 45, D353-D361 (2017).

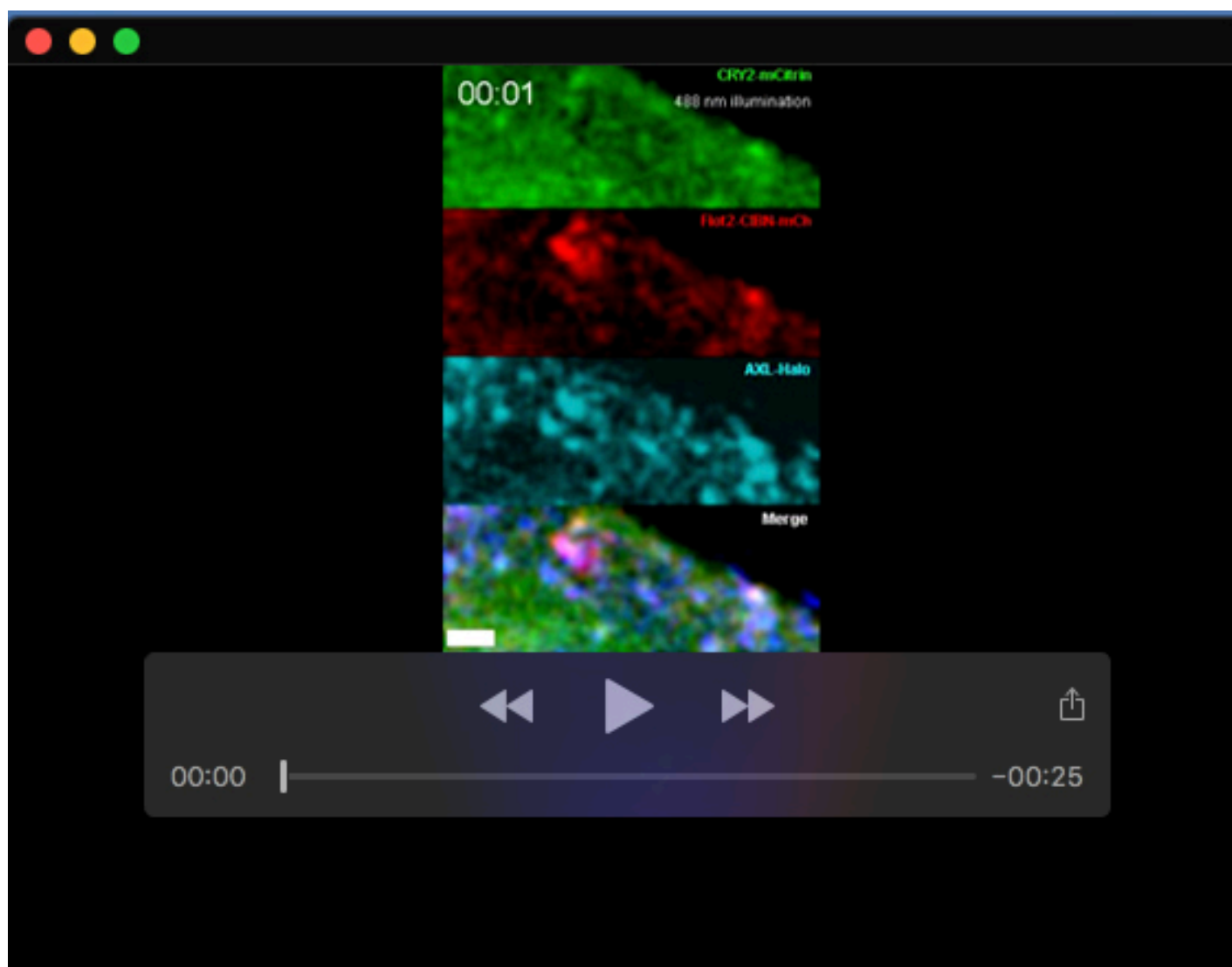
Kanehisa, M., Sato, Y., Kawashima, M., Furumichi, M., and Tanabe, M.; KEGG as a reference resource for gene and protein annotation. *Nucleic Acids Res.* 44, D457-D462 (2016).

Kanehisa, M. and Goto, S.; KEGG: Kyoto Encyclopedia of Genes and Genomes. *Nucleic Acids Res.* 28, 27-30 (2000).

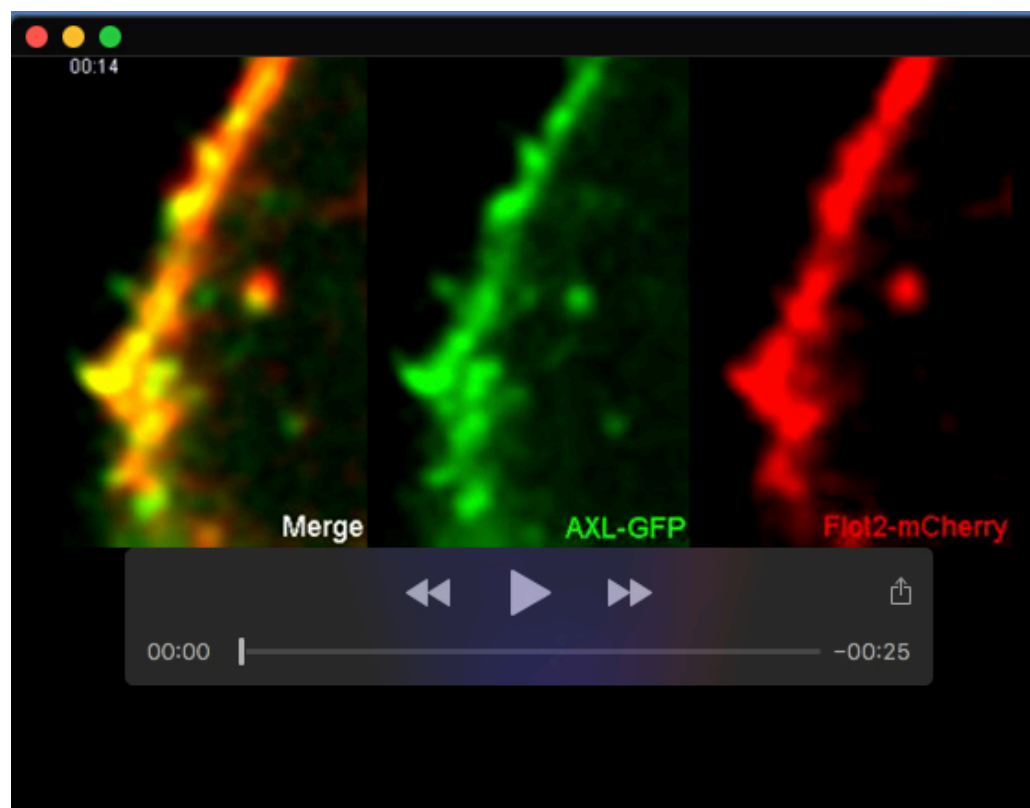
Genomatix

<http://www.genomatix.de/>

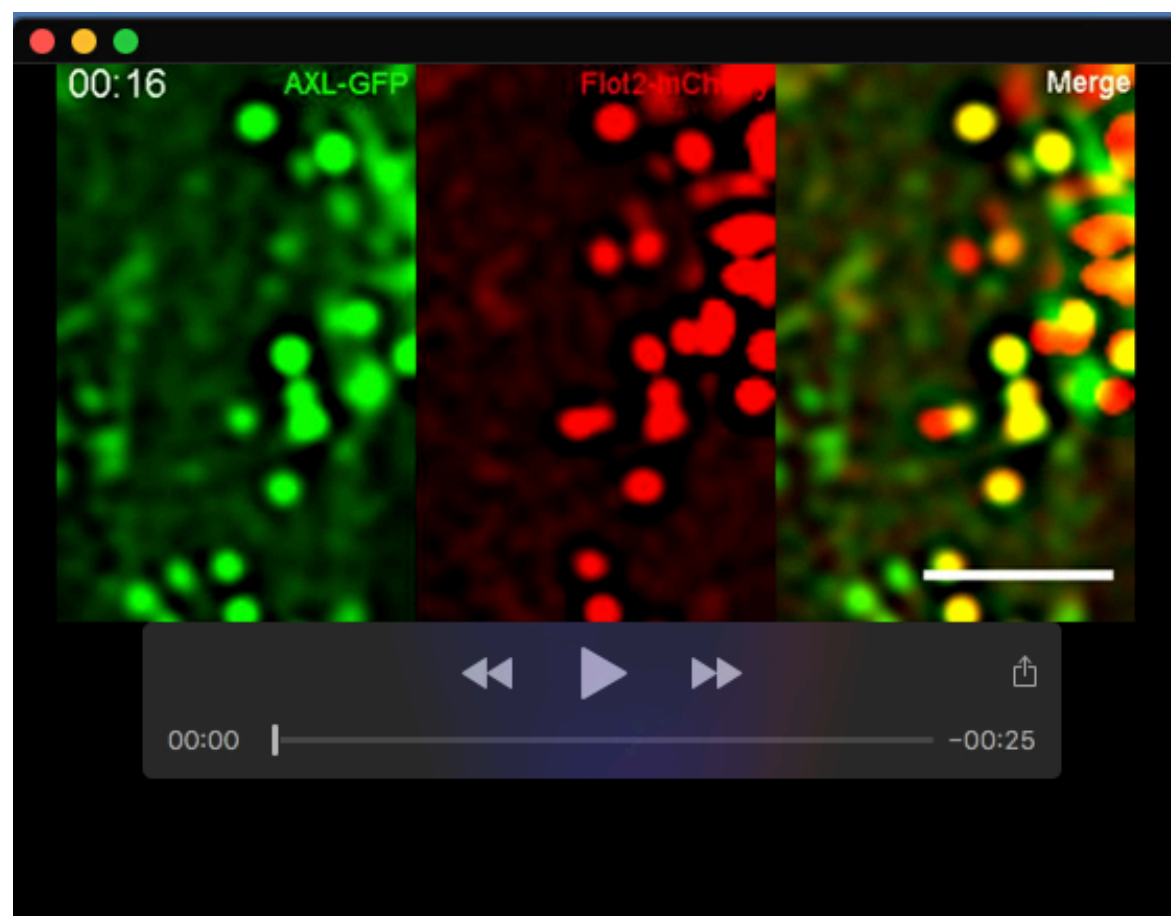
Genomatix Software suite version 3.10



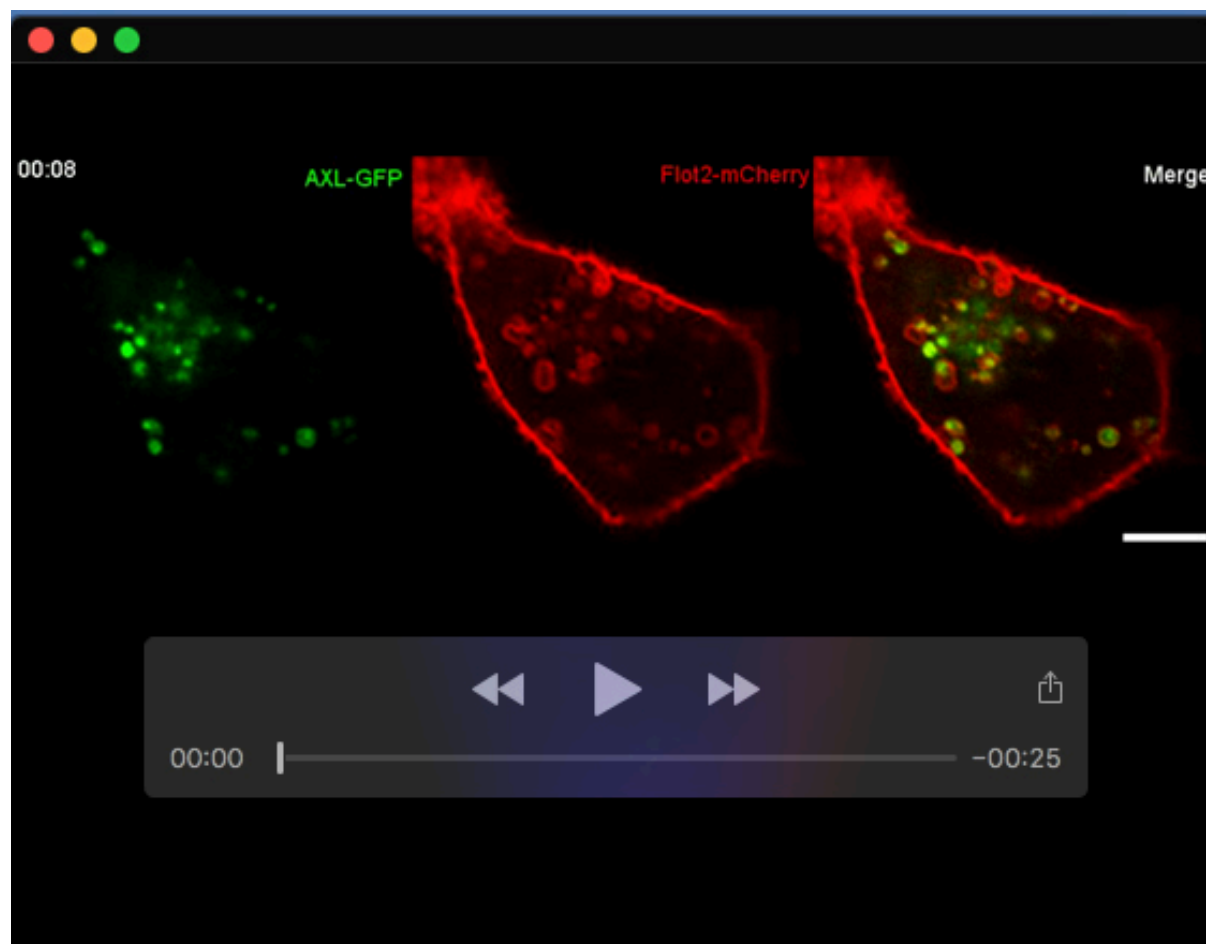
Movie 1. *Flotillin oligomerization induced by a CRY2-CIBN-based optogenetic approach promotes AXL co-clustering.* Movie of the boxed area from figure 4B. MCF10A cells that co-express CRY2-mCitrine (green), flotillin 2-CIBN-mCherry (red) and AXL-Halo (blue) labeled with Halo-Tag-Janelia Fluor 646 were imaged by TIRF microscopy. First, flotillin 2-CIBN-mCherry and AXL-Halo were imaged for 8 seconds before 488nm illumination. Then, cells were globally illuminated by 20 pulses (1 pulse/s, 100 ms time length for each) of 488nm-light to stimulate and visualize CRY2. During and after illumination, flotillin 2-CIBN-mCherry and AXL-Halo were continuously imaged. Two examples of flotillin 2/AXL-positive clusters induced by CRY2 oligomerization initiated by illumination are indicated (closed arrow). Co-localization events between flotillin 2-CIBN-mCherry and AXL-Halo are also visible independently of CRY2 oligomerization before illumination and correspond mostly to AXL-containing vesicles positive for flotillin 2 passing through the 200 nm depth of field illuminated by TIRF. Thanks to the high concentration of flotillin 2-CIBN-mCh in these vesicles, CRY2 translocation could be observed. Scale bar: 2 μ m.



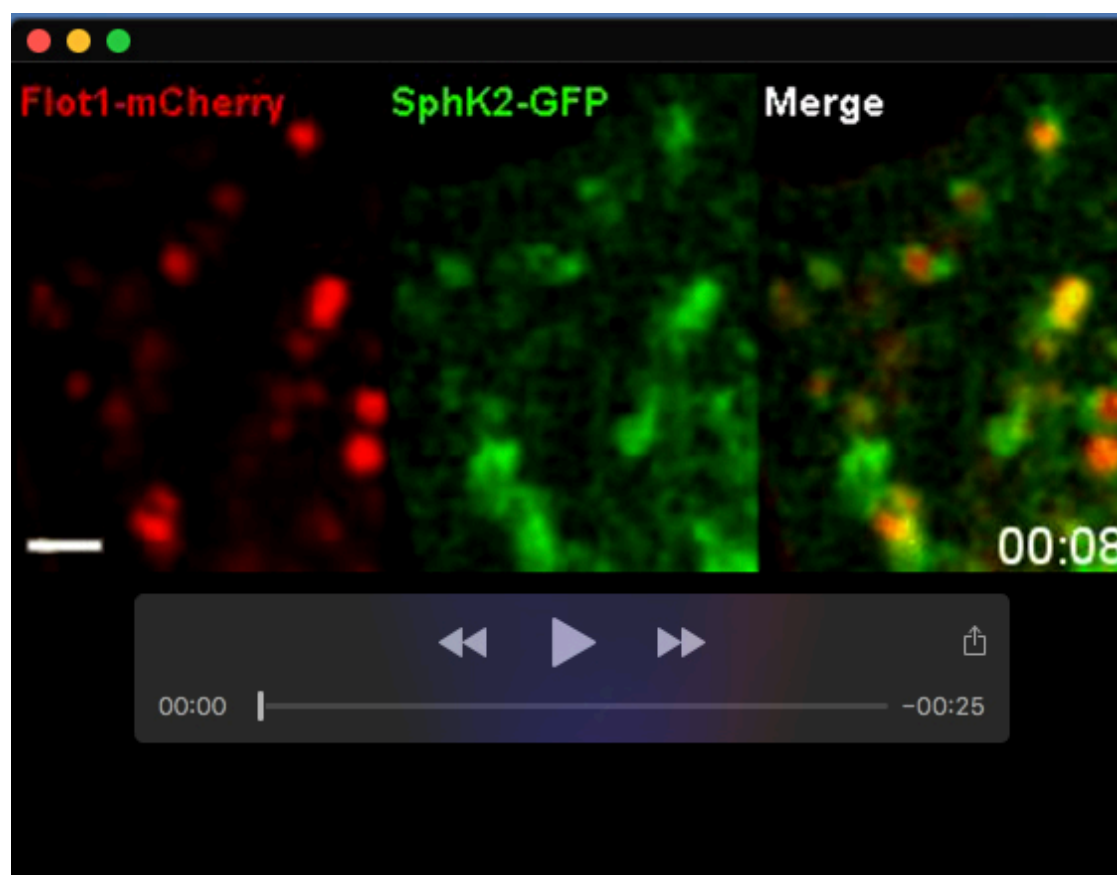
Movie 2. Co-endocytosis of flotillin 2 and AXL after their co-accumulation at the plasma membrane. MCF10AF1F2 cells that co-express flotillin 1-HA, flotillin 2-mCherry and AXL-GFP were imaged by spinning disk confocal microscopy (1 frame/1.3 s. Scale bar: 2.5 μm). Arrows indicate the site of co-accumulation of AXL and flotillin 2 and then the emerging endocytic vesicle.



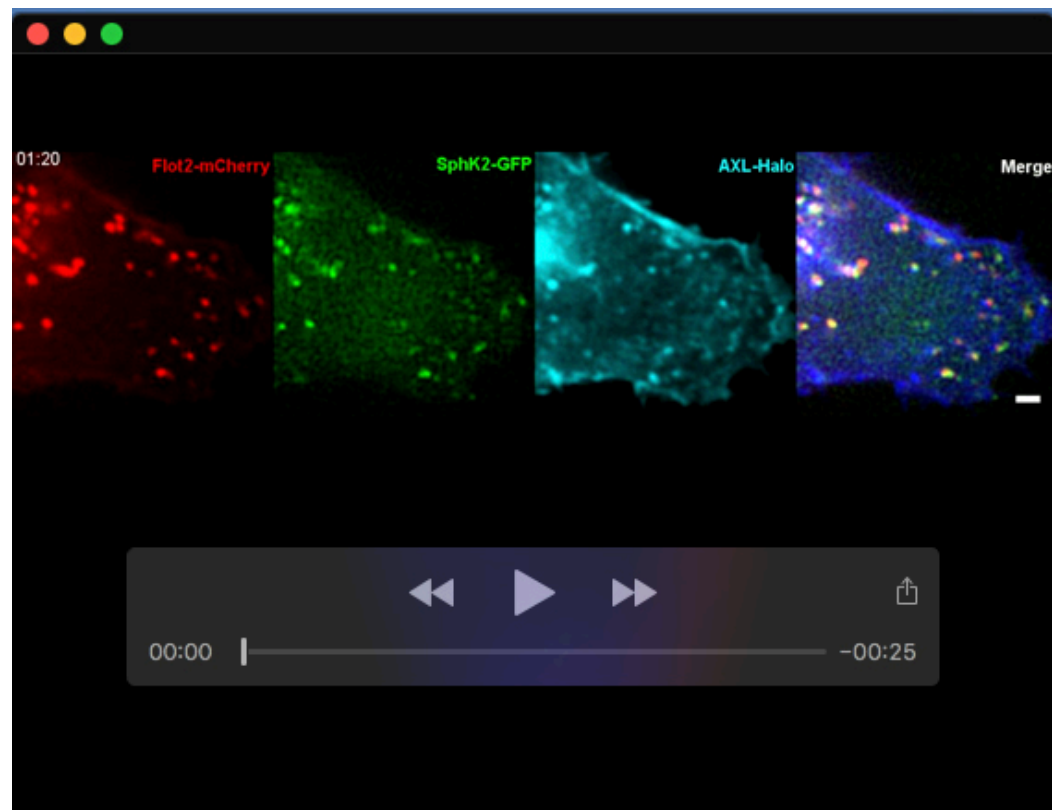
Movie 3. Flotillin 2 and AXL colocalize in intracellular vesicles. MCF10AF1F2 cells that co-express flotillin 1-HA, flotillin 2-mCherry and AXL-GFP were imaged by spinning disk confocal microscopy; 1 frame/1.3 s. Scale bar: 5 μm .



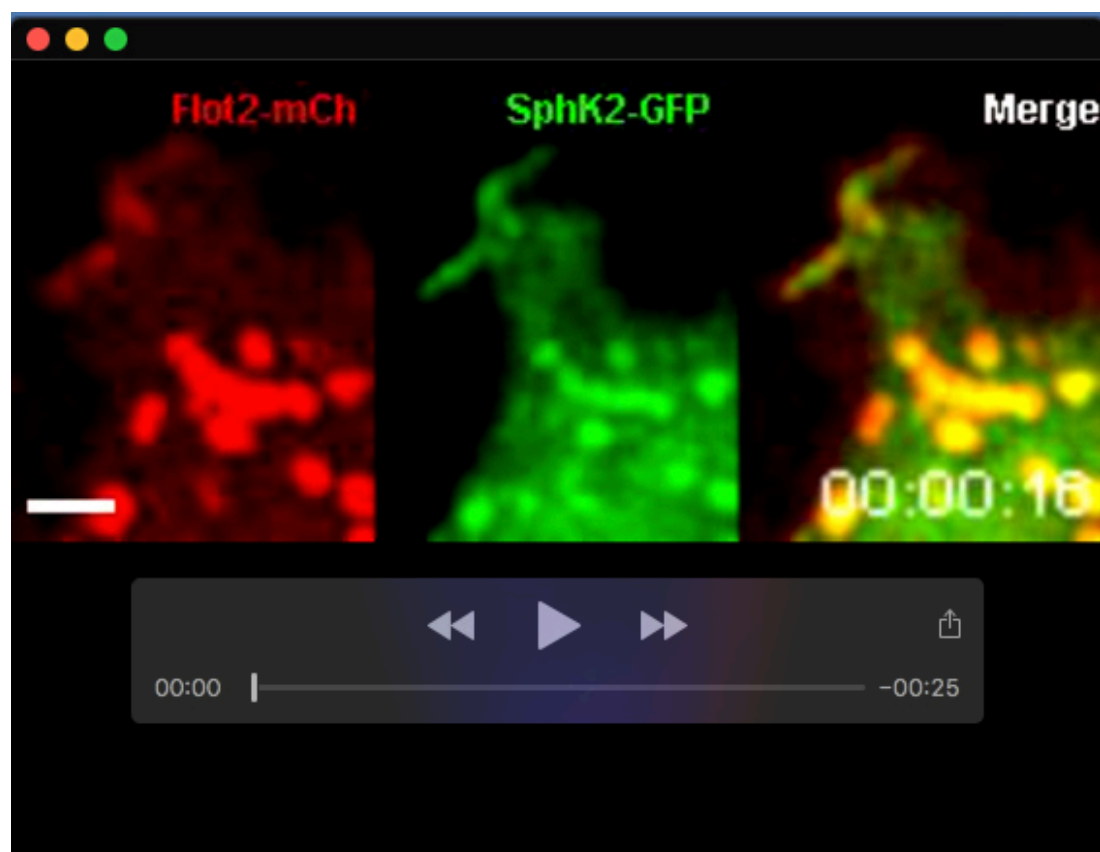
Movie 4. *Flotillin 2 and AXL colocalize in intracellular vesicles in tumor cells.* One MDA-MBA-MB-231 cell that co-expresses flotillin1-HA, flotillin-2-Cherry and AXL-GFP was imaged by spinning disk confocal microscopy; 1 frame/0.8 s. Scale bar: 10 μ m.



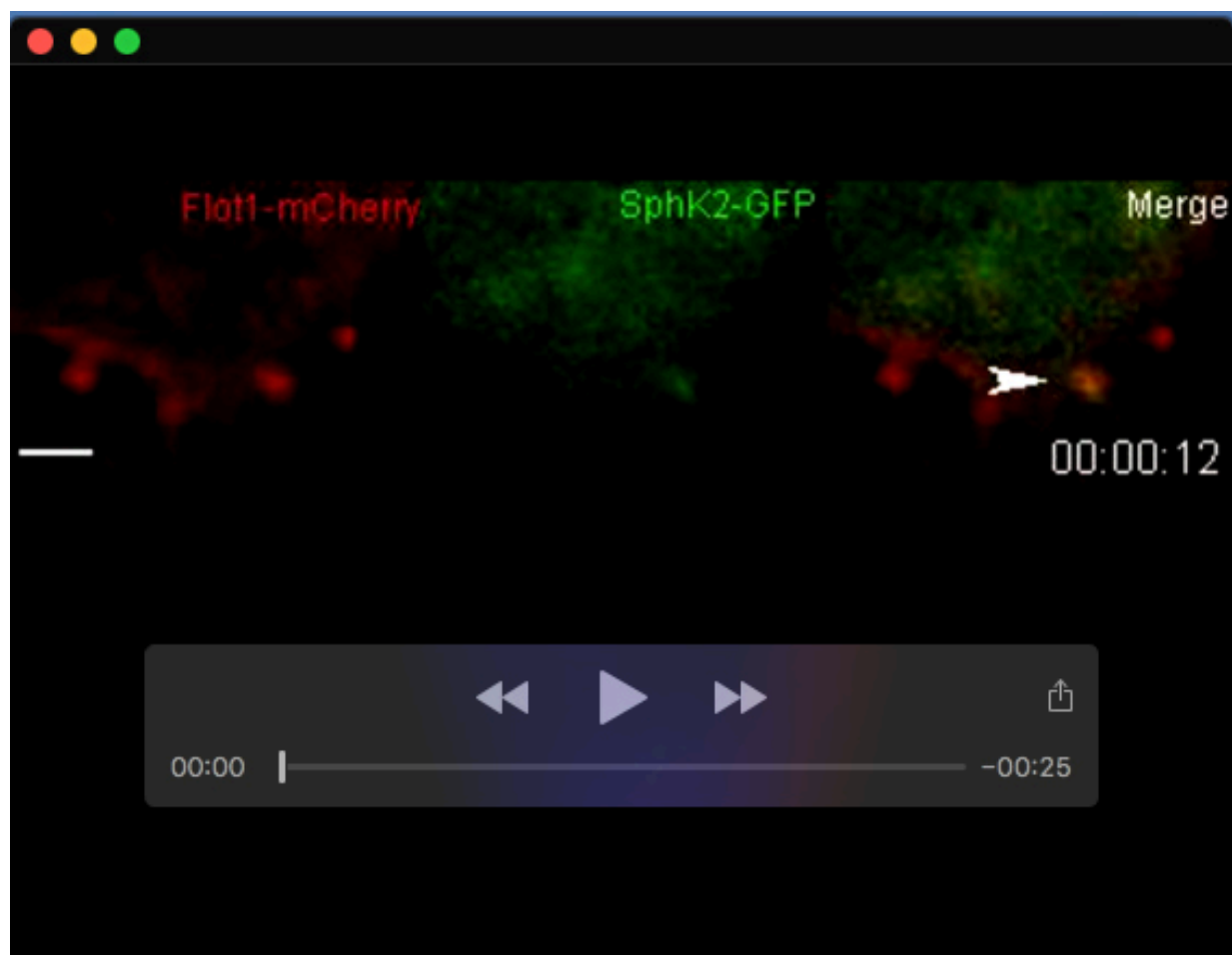
Movie 5. *SPHK2 is abundant in flotillin-positive late endosomes in MDA-MB-231 cells.* Movie of the boxed area shown in figure 5C acquired by spinning disk confocal microscopy of one MDA-MB231 cell that co-expresses flotillin 1-mCherry and SPHK2-GFP (1 frame/s. Scale bar: 2 μ m).



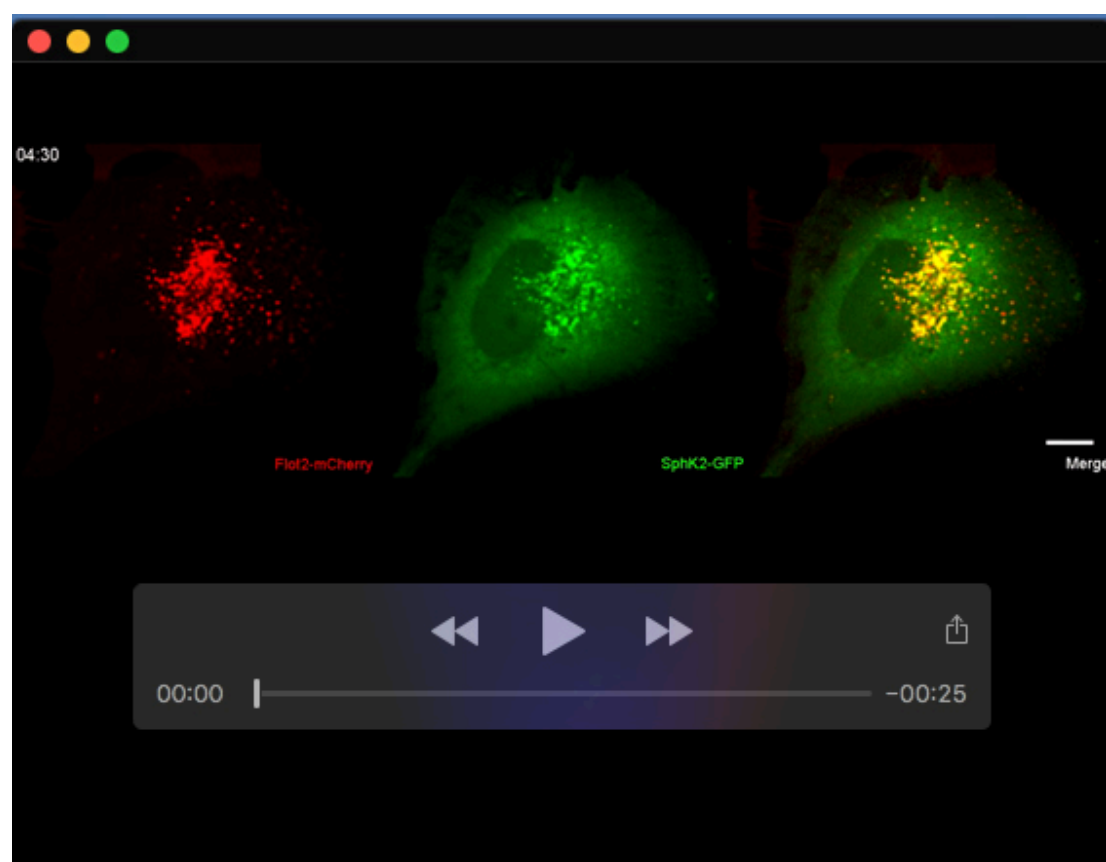
Movie 6. Co-localization and co-trafficking of AXL-Halo, SPHK2-GFP and flotillin 2-mCherry in one MCF10AF1F2 cell. Movie acquired by spinning disk confocal microscopy of one MCF10AF1F2 cell that co-expresses flotillin 2-mCherry (red), SPHK2-GFP (green) and AXL-Halo (blue) (labeled with Halo-tag-Janelia Fluor 646) (1 frame/10 s. Scale bar: 10 μ m).



Movie 7. Flotillin 2-mCherry/SPHK2-GFP co-endocytosis in MCF10AF1F2 cells. Movie of the boxed area shown in figure 5E (upper panel) acquired by spinning disk confocal microscopy of one MCF10AF1F2 cell that co-expresses flotillin 2-mCherry and SPHK2-GFP (1 frame/2 s). At 34s, arrows indicate sites of flotillin 2-mCherry and SPHK2-GFP co-accumulation at the plasma membrane followed by endocytosis of a vesicle positive for both proteins. (Scale bar: 2 μ m).



Movie 8. *Flotillin 1-mCherry/SPHK2-GFP co-endocytosis in MDA-MB-231 cells.* Movie of the boxed area shown in figure 5E (lower panel) acquired by spinning disk confocal microscopy of one MDA-MB-231 cell that co-expresses flotillin 1-mCherry and SPHK2-GFP. The arrow indicates the site of flotillin 1-mCherry and SPHK2-GFP co-accumulation at the plasma membrane followed by endocytosis of one vesicle positive for both proteins (1 frame/1 s). (Scale bar: 2 μ m).



Movie 9. *Inhibition of SPHK2 catalytic activity induces its delocalization from flotillin-positive endosomes.* One MCF10AF1F2 cell that co-expresses SPHK2-GFP was imaged by spinning disk confocal microscopy immediately after addition of Opaganib (50 μ M) (1 frame/30 s. Scale bar: 10 μ m). The disappearance of the SPHK2-GFP signal in flotillin 2-mCherry-positive vesicles is clearly visible after 8 min and lasted for the rest of the movie (up to 28.5 min).